land

MDPI

Article

Quantification of Amu River Riverbank Erosion in Balkh Province of Afghanistan during 2004–2020

Abdul Basir Mahmoodzada [1,2,*], Divyesh Varade [3], Sawahiko Shimada [2], Hiromu Okazawa [2], Shafiqullah Aryan [4], Gulbuddin Gulab [4], Abd El-Zaher M. A. Mustafa [5], Humaira Rizwana [5], Yogesh K. Ahlawat [6] and Hosam O. Elansary [7]

1 Faculty of Engineering Geology and Mines, Jowzjan University, Jowzjan 1901, Afghanistan
2 Department of Bioproduction and Environment Engineering, Tokyo University of Agriculture, Tokyo 156-8502, Japan; shima123@nodai.ac.jp (S.S.); h1okazaw@nodai.ac.jp (H.O.)
3 Department of Civil Engineering, Indian Institute of Technology Jammu, Nagrota 181221, India; divyesh.varade@iitjammu.ac.in
4 Faculty of Agriculture, Nangarhar University, Nangarhar 2601, Afghanistan; shafiqaryan@gmail.com (S.A.); malyargulab@gmail.com (G.G.)
5 Department of Botany and Microbiology, College of Science, King Saud University, P.O. Box 2455, Riyadh 11451, Saudi Arabia; amus@ksu.edu.sa (A.E.-Z.M.A.M.); hrizwana@ksu.edu.sa (H.R.)
6 Department of Biological Sciences, Michigan Technological University, Houghton, MI 49931, USA; ykahlawa@mtu.edu
7 Department of Plant Production, College of Food & Agriculture Sciences, King Saud University, P.O. Box 2460, Riyadh 11451, Saudi Arabia; helansary@ksu.edu.sa
* Correspondence: mahmoodzadabasir@gmail.com; Tel.: +93-786-271-272

Abstract: In this study, we propose quantifying the Amu River riverbank erosion with the modelled river discharge in Kaldar District, Balkh Province of Afghanistan from 2004 to 2020. We propose a framework synergizing multi-source information for modelling the erosion area based on three components: (1) river discharge, (2) river width, and (3) erosion area. The total river discharge for the watershed shared by Afghanistan and Tajikistan was modelled using hydrological parameters from the European Centre for Medium-Range Weather Forecasts (ECMWF) Reanalysis v5 (ERA5) data through multivariate linear regression with ground station data. The river width was determined manually using the Normalized Difference Water Index (NDWI) derived from Landsat data. The riverbank erosion area was derived from the digital shoreline analysis using the NDWI. The digital shoreline analysis showed that, between 2008 and 2020, the average riverbank erosion area in Kaldar District is about 5.4 km^2 per year, and, overall, 86.3 km^2 during 2004–2020 due to flood events. The significantly higher land loss events occurred at 10 km^2 bank erosion during the years 2008–2009 and 2015–2016, and 19 km^2 peak erosion occurred during 2011–2012. A linear relation between the erosion area with respect to the discharge intensity and the specific stream power was observed with an R^2 of 0.84 and RMSE of 1.761 for both.

Keywords: riverbank erosion; river discharge; NDWI; Landsat; ERA5

check for updates

Citation: Mahmoodzada, A.B.; Varade, D.; Shimada, S.; Okazawa, H.; Aryan, S.; Gulab, G.; Mustafa, A.E.-Z.M.A.; Rizwana, H.; Ahlawat, Y.K.; Elansary, H.O. Quantification of Amu River Riverbank Erosion in Balkh Province of Afghanistan during 2004–2020. *Land* **2023**, *12*, 1890. https://doi.org/10.3390/land12101890

Academic Editor: Guangju Zhao

Received: 11 September 2023
Revised: 26 September 2023
Accepted: 6 October 2023
Published: 9 October 2023

Copyright: © 2023 by the authors. Licensee MDPI, Basel, Switzerland. This article is an open access article distributed under the terms and conditions of the Creative Commons Attribution (CC BY) license (https://creativecommons.org/licenses/by/4.0/).

1. Introduction

Riverbank erosion and shoreline changes are the most significant geomorphological environments and natural disasters in several parts of the world [1,2]. Subsequently, several studies have investigated landform dynamics, riverbank erosion, and floods and their impact on society [3–7]. Riverbank erosion is also significant from the perspective of socio-economic aspects due to the loss of agricultural land adjacent to the river channel [3,8–11]. Such phenomena are even more significant for transboundary nations such as Afghanistan and Turkmenistan, whose national boundaries, to some extent, are determined by the Amu River [12,13]. Numerous factors have been known to affect the riverbank erosion over time, including the flow conditions, precipitation, soil composition, soil moisture, temperature

conditions, and snowmelt dynamics for glacial rivers [14–17]. Flooding and riverbank erosion are often also caused by a combination of sharp slopes upstream with associated heavy rainfall and snow-glacier melt [18–21]. Moreover, denudation of unstable parts of the mountains and lack of vegetation further contribute to the issues related to flooding and riverbank erosion [22–24].

The Amu River elevation between Badakhshan and Kham Ab has more than a 5000 m difference as every year, due to flash floods, about 250 million m^3 of sediments are transported through riverbank erosion of large areas of Afghanistan [25,26]. Flash flooding and riverbank erosion are concurrent events where mostly the flood and riverbank erosion co-occur or a flood is sequentially followed by riverbank erosion [18,27]. In Afghanistan, flash floods most frequently occur in March and follow until May because of heavy rainfall. During June–July, flooding mainly occurs due to the snowpack and glaciers melting in the Pyanj–Amu River Basin. The Pyanj–Amu River Basin runs for 2400 km in length and has an area of 90,716.7 km^2, with a large number of tributaries in central Asia, but it dries up in the Tura lowlands in Turkmenistan and Uzbekistan [10,28].

The continuous availability of the ERA5 Reanalysis data enables monitoring of hydrological parameters over large watersheds, such as the Khanabad watershed [29,30]. In the absence of well-distributed ground stations, ERA5 Reanalysis data have been widely utilized for hydrological modeling [31]. Considering transboundary watersheds, the ERA5 Reanalysis data have been proven to be highly significant for hydrological modeling [29,32]. The purpose of this study is to quantify the riverbank erosion in Kaldar District, Balkh Province of Afghanistan. For the investigation, we utilized a combination of ground station data available from the Afghanistan side and ERA5 Reanalysis data [33]. A multivariate regression model is developed using the investigated hydrological parameters from the ERA5 Reanalysis data to estimate the overall river discharge for the entire watershed shared by northern Afghanistan and Turkmenistan. The modeled discharge is analyzed with respect to the manually determined river width using the Landsat-7/8 multispectral datasets, and further flow parameters are determined, which are linked to the riverbank erosion estimated using shoreline analysis. The investigation was carried out from 2004 to 2020.

2. Materials and Methods

2.1. Study Area

The investigated area is a shared basin between two counties, with the southeast part located in Afghanistan and the northern part in Tajikistan, and covers significant elevation changes ranging between 230 and 7500 m a.s.l, as shown in Figure 1. The Amu River originates from the high snow-covered altitudes of the Pamir Hindu Kush Himalayas. The Amu River flows along the border between Afghanistan and Tajikistan, Uzbekistan, across Turkmenistan, and returns to Uzbekistan, where it discharges into the Aral Sea [12]. From its entry into Badakhshan Province to its confluence with the Aral Sea, the channel length of the Amu River is about 2500 km. Out of the total river length, 1200 km of the river is located between Afghanistan across the border with Tajikistan, Uzbekistan, and Turkmenistan [34]. The drainage area of the Amu River basin is about 219,112.27 $km^{2,}$, of which only 90,716.7 km^2 is located in Afghanistan (Figure 2), with the remainder in Tajikistan. Afghanistan occupies the higher altitudes in the upper Amu River basin, extending from the Pamir Hindu Kush regions of Badakhshan Province and continuing in the lower altitudes of the Kham Ab District of Jawzjan Province, as shown in Figure 2. The upper Amu River basin comprises an intricate network of nine prominent streams, as shown in Figure 2, with Pyanj and Vaksh River streams as the significant contributors [35].

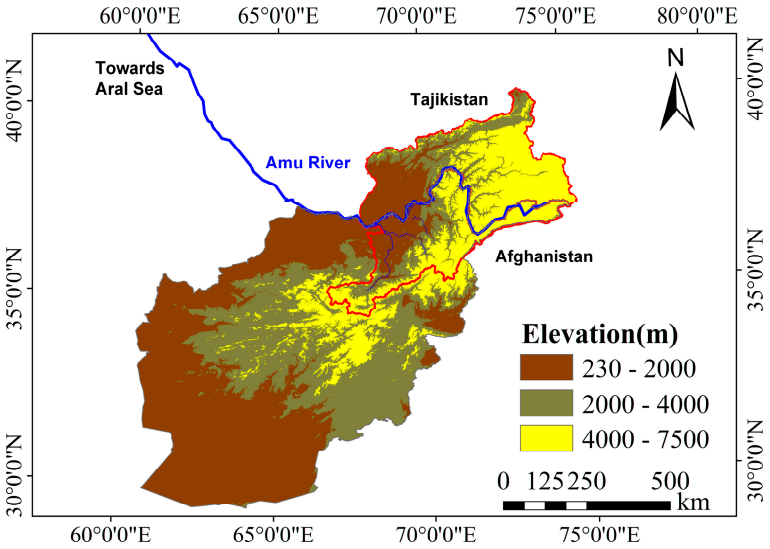

Figure 1. Khanabad watershed covering regions of Afghanistan and Tajikistan with categorized elevation determined from SRTM 1 arc sec Digital Elevation Model (DEM). The Amu River in blue originates from very high elevation areas and flows west towards the Aral Sea.

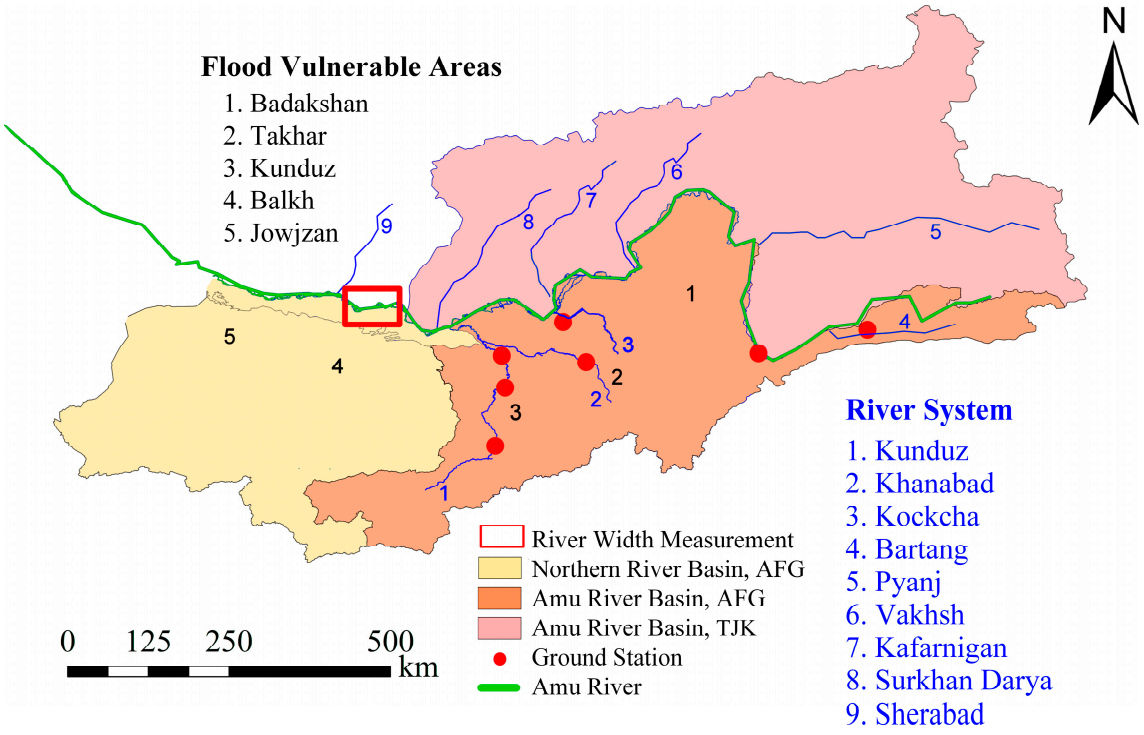

Figure 2. Investigation area for Amu River shifting and riverbank erosion in Kaldar District of Balkh Province, Afghanistan, shown under the red box. The different streams contributing to the Amu River are shown in blue, with ground stations for river discharge data.

Afghanistan is an arid country that receives relatively little rainfall; thus, the snowmelt from mountains in the north plays a crucial role in providing water resources. Precipitation usually occurs in the winter as snowfall, while rainfall events are typically observed in spring and summer with an overall dominance of snowfall over rain towards contribution to the water resources. Snowmelt occurs as temperature rises in the spring and the summer (Figure 3a). At the same time, in the spring, rapid snow melting contributes to flooding and subsequent riverbank erosion along the Amu River on the Afghanistan side. The riverbank

erosion is more prominent on the Afghanistan side due to the topography and the lack of adequate measures for mitigation [12].

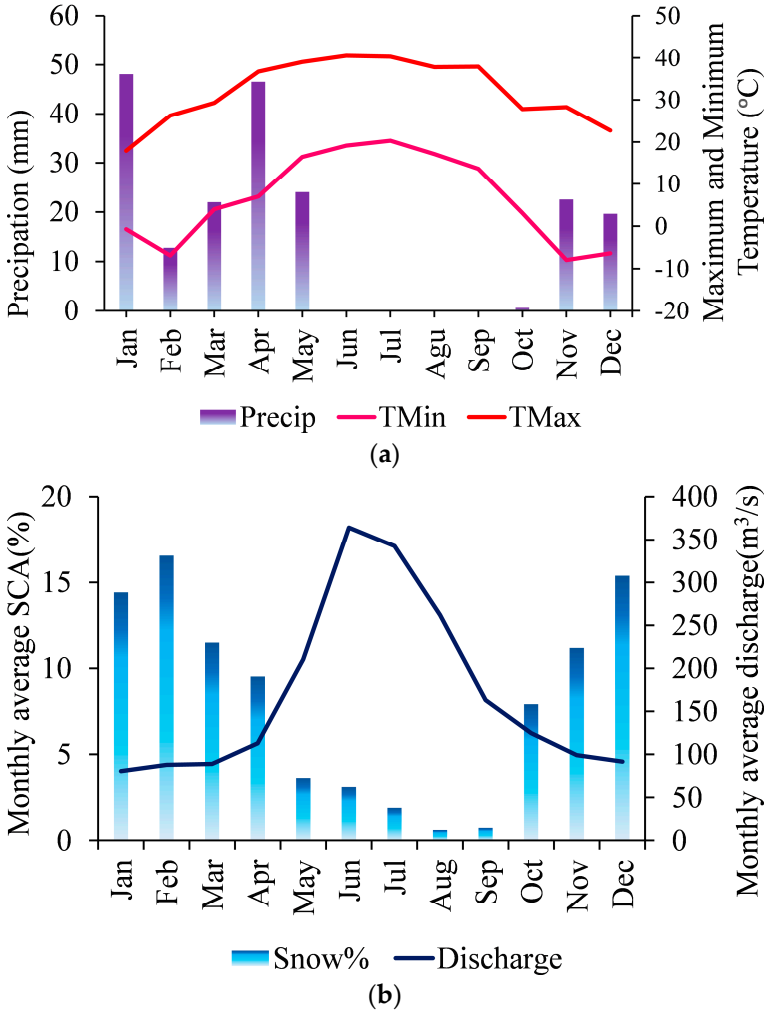

Figure 3. (**a**) Annual precipitation–snowmelt–temperature cycle in the Amu River basin; (**b**) annual snowmelt and discharge cycle.

Generally, flooding occurs due to excessive heavy rainfall or snowmelt from the higher elevated area of Pamir Hindu Kush mountains. The consequence of heavy rainfall is flash flood, which causes destruction of the property and agricultural lands due to the channel shifting of riverbank erosion downstream. The prominently vulnerable provinces to floods in Afghanistan are Badakshan, Takhar, Kunduz, Balkh, and Jowzjan Provinces [28], as shown in Figure 2. The study area includes the snow-covered and glacierized sub-basins within the Pamir and Hindu Kush mountains of Afghanistan and Turkmenistan. The headwaters are primarily monitored at Pyanj River and at other streams in the headwaters of the Vakhsh River (Figure 2). The Pyanj and Vakhsh Rivers receive water from snowmelt from most of the snow cover area in the watershed [36,37]. A maximum river discharge is typically observed in the spring and summer, contributed from the snowmelt, and, in fall, the river discharge reduces and comprises contributions from the glacier melts. The river discharge is usually at the lowest during winter, as shown in Figure 3b.

2.2. Test Datasets

European Center for Medium-Range Weather Forecasts (ECMWF) produces reanalysis products in the form of gridded data, typically at 9 sq. km spatial resolution. The data result from numerical weather prediction models with observations from various satellites

and ground stations [29]. Mahto and Mishra investigated the potential of ERA5 data for hydrological applications in India and observed the performance of ERA5 to be relatively better than other reanalysis datasets [32]. Tarek, Brissette, and Arsenault [29] demonstrated that, as compared to ERA-Interim, the ERA5 Reanalysis products are systematically more accurate. It is evident that ERA5 Reanalysis data have been efficiently used for hydrological studies [29,31,34,38]. In the present study, to account for the unavailability of ground station observations from the Tajikistan side of the Khanabad watershed, ERA5 Reanalysis data were used for hydrological modeling. For this, several hydrological parameters discussed in the next section were used for February to July from 2004 to 2020. The later months were excluded from this study on account of the lesser influence of the river dynamics on the riverbank erosion. Remotely sensed data have been widely used for the mapping of riverbank erosion and morphological dynamics of rivers [39–42]. The multispectral data from the Landsat mission have provided significant means for understanding the morphology of the rivers [43,44]. For extracting the morphology of the Amu River during the 16 years, Landsat images (TM/ETM/OLI TRI) from 2004 to 2020 were considered for the analysis.

2.3. Methods

The riverbank erosion is generally governed by flow parameters such as the discharge intensity (DI) and the specific stream power (SSP), which are a function of the river discharge (Q) and the river width [45]. For a large watershed, as in the present study, determining effective discharge requires a large number of ground stations, which are usually scarce. Subsequently, the applicability of other datasets, such as the ERA5 Reanalysis datasets, is significant in such scenarios. We analyzed the agreement between the mean river discharge (Q) from the available ground stations from the General Directorate of Water Resources, National Water Affairs Regulation Authority (GMSGA), Afghanistan, and the various hydrological parameters determined from ERA5 Reanalysis data, as shown in Table 1. In Table 1, the correlation coefficient was determined for the parameters for the period of 2008–2018 from February to June as the river discharge data were available from 2008–2018. The months from July to January were excluded on account of the fact that the discharge in these months is relatively much lower and is mostly dominated by glacier melt, particularly in later months. A generalized flowchart for the adopted methodology is shown in Figure 4, where the two blocks represent the two phases of the investigation.

Table 1. Correlation between the mean river discharge and the ERA5 Reanalysis hydrological parameters for a period of 2008–2018 for months February to June.

S. No	ERA 5 Reanalysis Variable Names	Units	Description	Correlation Coefficient
1	rsn	kg m^{-3}	Snow density	0.99
2	sd	m of water equivalent	Snow Water Equivalent	0.99
3	sde	m	Snow depth	0.99
4	sf	m of water equivalent	Snowfall	0.69
5	smlt	m of water equivalent	Snowmelt	0.92
6	ssro	m	Sub-surface runoff	0.90
7	sro	m	Surface runoff	0.83
8	ro	m	Runoff	0.84
9	tp	m	Total precipitation	0.81

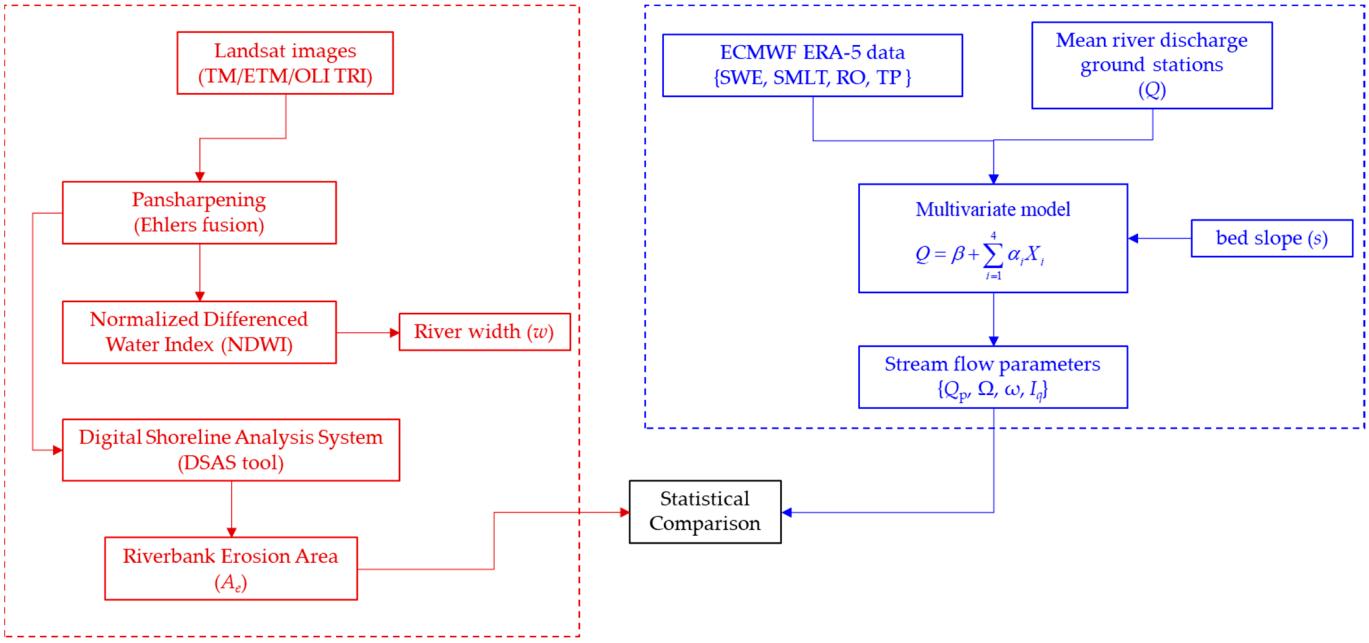

Figure 4. Generalized workflow describing the proposed methodology for investigating the riverbank erosion and its correspondence with the stream flow parameters.

We estimated the river discharge from a multivariate regression model shown in Equation (1), where the independent variables are determined from the hydrological parameters (SWE, SMLT, RO, TP) available from the ERA5 Reanalysis data. For this purpose, we utilize the mean discharge from the ground stations as the dependent variable shown in Figure 1b.

$$Q = \beta + \sum_{i=1}^{4} \alpha_i X_i \quad (1)$$

where i = 1,2,3 and 4 corresponds to the sequence of the parameters snowmelt (SMLT), Snow Water Equivalent (SWE), Runoff (RO), and Total Precipitation (TP), respectively, and X denotes these parameters. In Equation (1), α represents the coefficients for the aforementioned parameters, and β is a constant. The multivariate linear least squares regression yielded values $\alpha_1 = -86.105$, $\alpha 2 = 0.172$, $\alpha_3 = 188.724$, $\alpha_4 = 60.479$, and $\beta = -86.1054$, with an adjusted coefficient of determination of 0.99 and an RMSE of 15.28 m^3/s for the modeled river discharge.

The river width (w) was determined in the regions located in the Kaldar District of Balkh Province across the Amu River between Afghanistan and Uzbekistan, which is at an approximate distance of 36 km from the collective assimilation of the various stream flows in the Amu River, as shown in Figure 2. The river width was manually determined from the Normalized Difference Water Index (NDWI) derived from the Landsat-7 and Landsat-8 multispectral datasets [34,46]. The Landsat images were pan-sharpened using the Ehlers fusion method [47] to improve river width measurement quality to 15 m spatial resolution before generating the NDWI images. The Ehlers fusion is employed to ensure higher details in the multispectral images while preserving the spectral attributes during the fusion process [48,49]. A mean of five adjacent manual observations of approximately 100–200 m apart from the NDWI image was used for the river width. In the case of Landsat 7, the scan line corrector was utilized for gap filling [50].

Additionally, the Landsat images were also used to determine the riverbank erosion area (A_e) based on the digital shoreline analysis [12]. River lines (edges) were digitized to collect shoreline layers from individual images annually. Digital shoreline analysis system (DSAS) was used for baseline measurement and calculation of the statistical change rate from the time series of shorelines and the corresponding erosion area [12]. DSAS creates

transect lines perpendicular to the reference line, i.e., baseline, at a user-specified distance interval [51]. The stream power or the total stream power (Ω) represents the loss of potential energy of the river against the riverbed and the riverbank, as defined in Equation (2).

$$\Omega = \gamma Q s \tag{2}$$

where γ is the specific weight of water (equivalent to the product of density of water 1000 kg/m^3 and the gravity 9.8 m/s^{-2}), and s is the riverbed slope.

The specific stream power (ω) is defined as the total stream power per unit width, i.e., (Ω/w). The discharge intensity (here, I_q = Q/w) and ω are determined using the estimated river discharge (Q_p) from Equation (1) and the approximated river width [45]. For the determination of the specific stream power, the bed slope (s = 2.7) was calculated as the ratio of rise and run approximated using the data provided by Akbary [52] as the measurements of the riverbed elevation were not available.

3. Results and Discussion

3.1. Snowmelt or Precipitation Dominance on Amu River Discharge

The annual precipitation cycle in the Amu River basin was discussed earlier in Section 2.1, where the precipitation is high during January–March and after that declines. Based on the ERA5 Reanalysis data, we investigated the dominance of the snowmelt over precipitation or vice versa for runoff contribution. Figure 5 shows the scatterplots between these parameters for February to June from 2004 to 2020. The snowmelt is represented in the meters equivalent of water corresponding to the total accumulated amount of water that has melted from snow in the gridded snow-covered area. The total precipitation comprises the large-scale sum of precipitation and convective precipitation including rain and snow falling to Earth's surface.

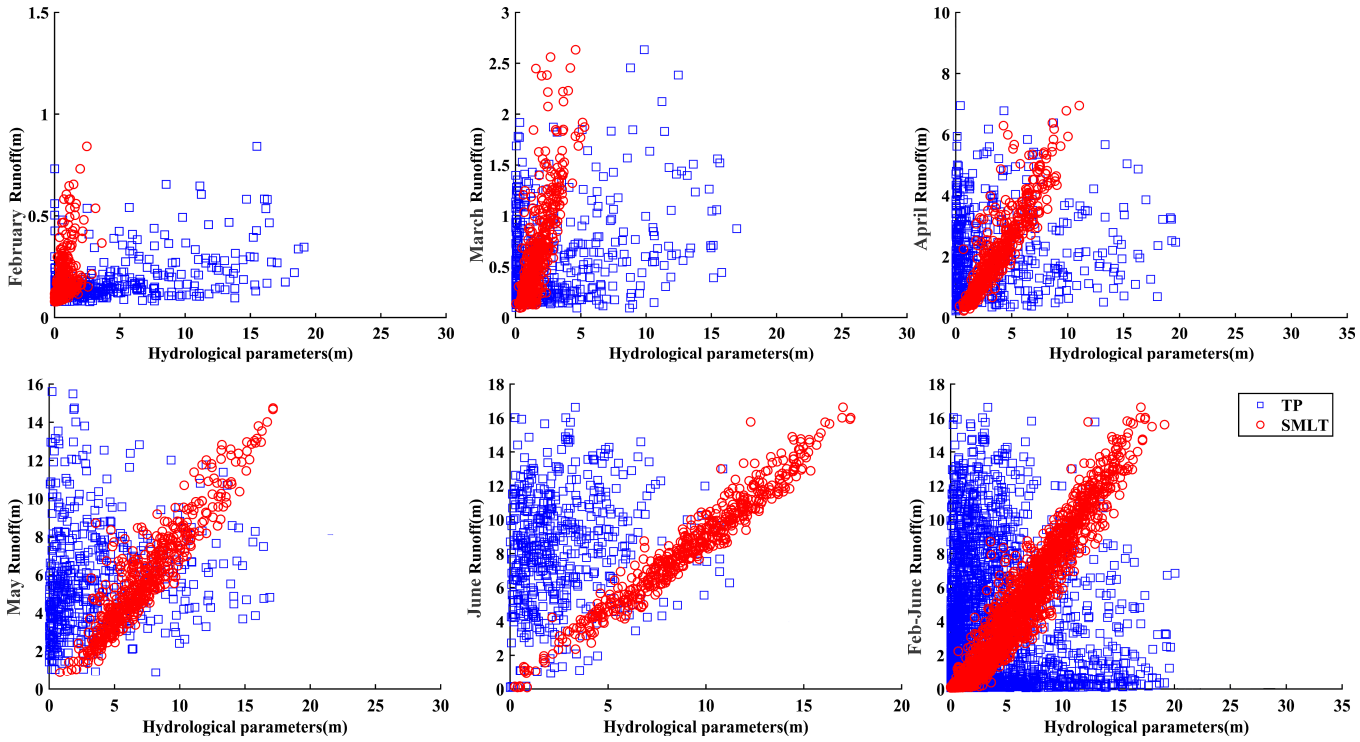

Figure 5. Month-wise snowmelt (SMLT) in red, and total precipitation (TP) in blue versus runoff scatter from 2004 to 2020 for February, March, April, May, and June.

From Figure 5, it is observed that the monthly precipitation shows a rather inconsistent distribution as compared to the snowmelt. From February to April, the precipitation is

observed to dominate the contribution to the runoff. In contrast, snowmelt dominates the contribution to the runoff for May and June, with a steady increase leading to a corresponding increase in the runoff. The runoff in February and May is relatively more prominent than in the other months. However, from June onwards, the runoff decreases significantly.

The proportional distribution of the snowmelt, the total precipitation, and the runoff for a block period of five years are shown in Figure 6, showing similar trends as in Figure 5, where the runoff is much lower in winter and increases in summer, possibly attributed to the rise in temperatures leading to increased snowmelt. For showing the comparison between the proportional distribution of the snowmelt and total precipitation, these parameters are normalized and weighted with respect to their sum. The runoff in Figure 6 is also normalized. The contribution of snowmelt to the runoff is also expected to be higher than precipitation. It is observed that the proportions of snowmelt are consistently higher than precipitation for the block period of years, as indicated in Figure 6.

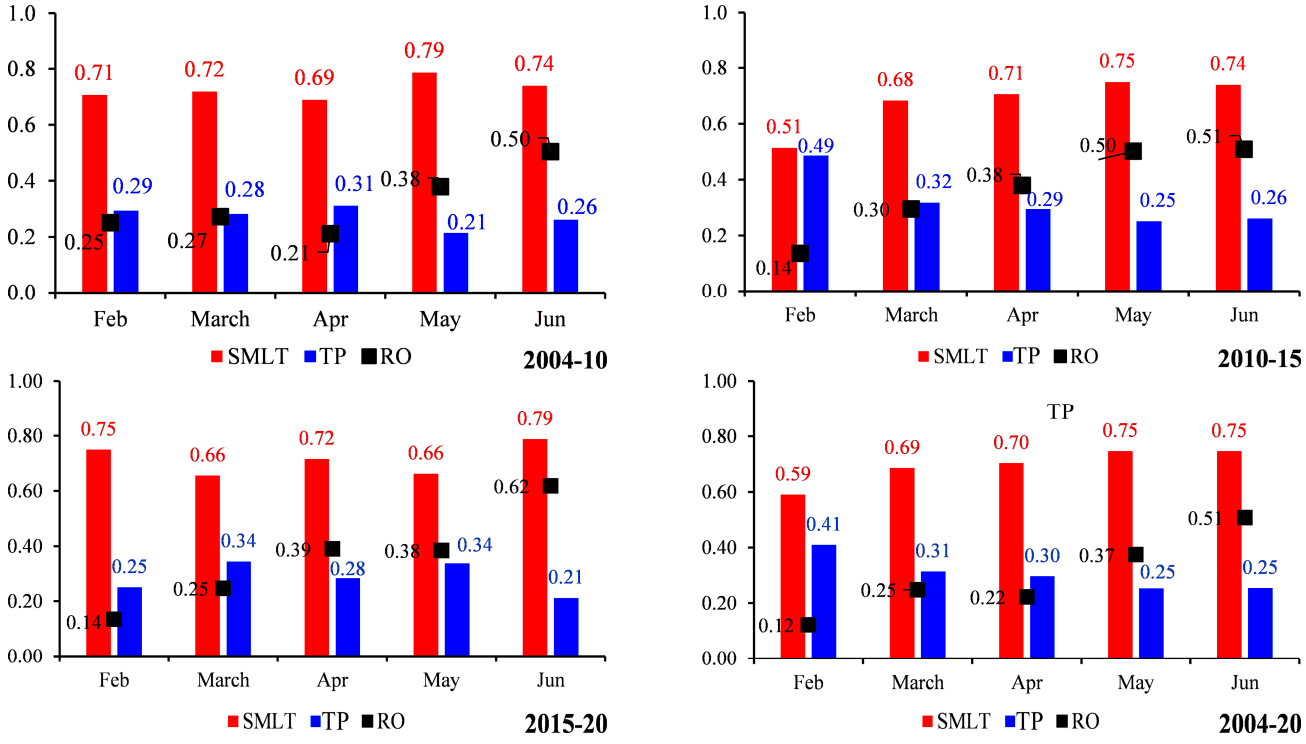

Figure 6. The mean normalized runoff (RO) is shown as black squares, and the proportions of normalized snowmelt (SMLT) in red and total precipitation (TP) in blue for the months of February to June over a block period of years.

A gap between the snowmelt and precipitation proportions is observed between 2010 and 2015 during March (Figure 6). Badakshan, Takhar, and Baghlan Provinces have been observed to be highly vulnerable to flooding events, particularly between the years 2012–2015, according to the data disseminated by the United Nations Office for the Coordination of Humanitarian Affairs [53,54]. According to Climate World Bank [55], in the years following 2009, an unprecedented increase in the mean rainfall was observed in these provinces and also in Tajikistan, leading to the reduced gaps between the snowmelt and the total precipitation as observed for March in Figure 6. This gap could possibly be due to extreme torrential rainfall events, which resulted in several flooding events during these years. Further, according to the International Disaster Database, a major riverine flood occurred in Badakshan District in Afghanistan on 4 February 2013 due to continuous heavy rainfall [56]. The higher contribution of snowmelt to the runoff as compared to rainfall was also observed in several other studies, particularly in the Italian Alps [57]. For the central Spanish Pyrenees, López-Moreno and [58] also demonstrated that the snowmelt

contributes more to the discharge than rainfall in spring. In another study by Fassnacht and Records [59], snowmelt was regarded as a more significant parameter than precipitation and rainfall frequencies to explain the flood frequencies in mountainous regions.

3.2. Linkage between the Flow Parameters and the Amu River Riverbank Erosion

Although numerous factors affect riverbank erosion, including the soil characteristics and the hydrological flow parameters, periodical information retrieval of the soil strength is not possible; thus, most studies rely on the assessment of hydrological flow parameters of the river for the analysis of corresponding riverbank erosion. In the present study, we utilized the hydrological parameters from the ERA5 Reanalysis data to predict the river discharge for 2004–2020. It was observed that the predicted discharge follows a power law relation with the manually determined river width using the NDWI derived from the Landsat mission data, as shown in Figure 7a. The correlation is carried out based on a robust non-linear model to account for the uncertainties arising in the river width on account of various factors, such as the angle of attack of the river to the bank at sharp curves or bends and other influencing factors, including anthropogenic activities. Some of the points below the 95% confidence bounds in Figure 7a could be attributed to the drought periods that occurred during 2006–2008, as indicated by UNOCHA [60]. A similar strategy was followed to link the annual riverbank eroded area (m^2) determined from the shoreline analysis and the flow parameters, including the discharge intensity, stream power, and the specific stream power.

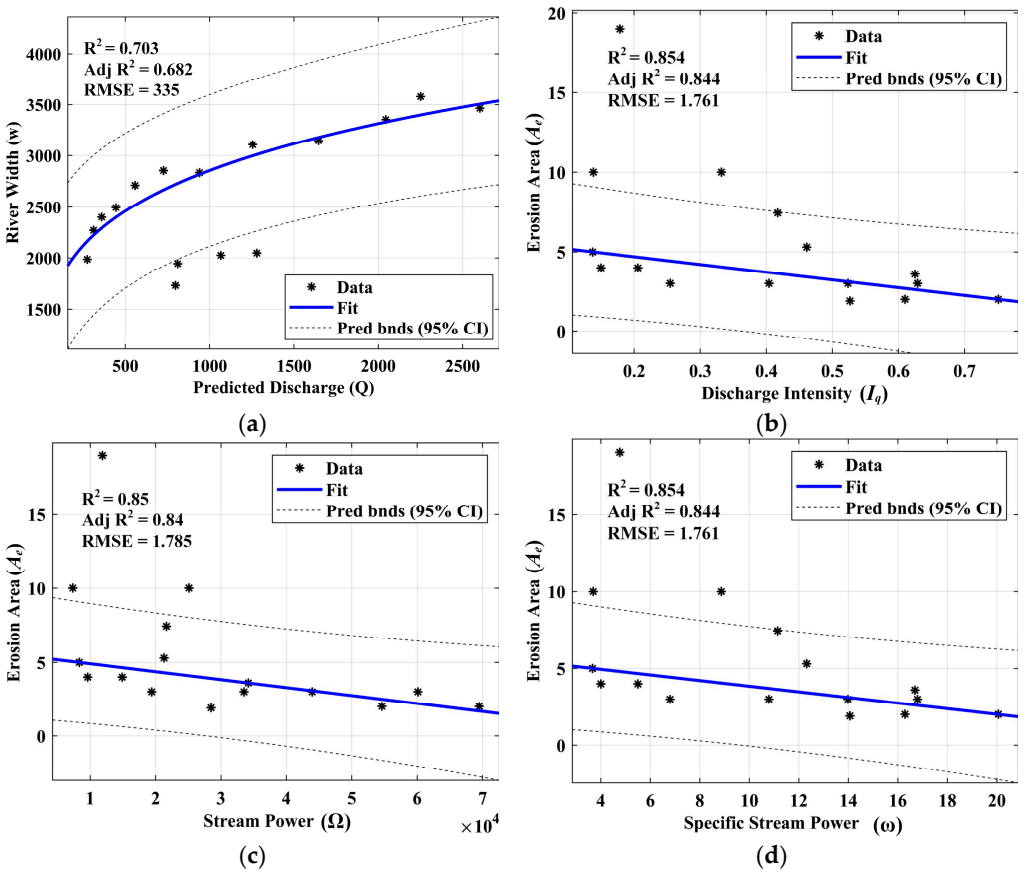

Figure 7. (**a**) Robust power law fit between the river width and predicted discharge; (**b**) robust linear fit between the riverbank erosion area and the discharge intensity; (**c**,**d**) show the robust linear fit between the riverbank erosion area and stream power, and between riverbank erosion area and the specific stream power.

Overall, it was observed that the robust linear fit based on the least-squares method yielded a very good correlation between the eroded area and the flow parameters—DI, SP, and SSP. The statistical parameters of the comparison between the erosion area (Ae) and the flow parameters are shown in Table 2. It is worth mentioning that the points outside the 95% confidence bounds in each of Figure 7b–d correspond to peak events of the riverbank erosion during the years 2009, 2012, and 2015, which experienced several disasters due to flash floods and riverine floods that are possibly not estimated accurately in the present study. This error is possibly due to the fact that we utilized the data from the available ground stations located only on the Afghanistan side of the study area to predict the river discharge from the ERA5 Reanalysis data. However, extreme rainfall events during these periods were observed in the Takhar and Baghlan regions, where the river enters the flood plains, corroborating the peak events of riverbank erosion.

Table 2. Statistical comparison of the flow parameters with respect to the erosion area.

Comparison	Correlation Coefficient (R)	Coefficient of Determination (R2)	Coefficient of Determination (Adj R2)	Root Mean Square Error (RMSE)
w vs. Qp	0.8385	0.7031	0.6819	335.4
Ae vs. Iq	0.9241	0.8539	0.8435	1.761
Ae vs. Ω	0.9241	0.8539	0.8435	44.6
A_e vs. ω	0.9241	0.8539	0.8435	1.761

3.3. Periodical Land Loss Due to Amu River Riverbank Erosion

Afghanistan is one of the highly vulnerable countries to natural disasters such as floods, which often also cause erosion of precious land, property, and infrastructure. Land loss due to riverbank erosion has been a significant issue in Afghanistan, hindering its overall economic growth, as reported by [34,61]. Evidently, these erosion events often cause the shifting of rivers and river width to increase and are mostly governed by factors such as river discharge.

In the present study, the predicted mean river discharge shows a non-linear increasing trend where an early decrease occurred in the periods of 2006–2008, which were significant drought periods in Afghanistan. However, the river width is observed to show a consistent linearly increasing trend (Figure 8a), which is understandable as any soil lost during erosion is not replenished in the downstream areas. It is worth mentioning that the river width measurements were made in the regions where the Amu River enters the flood plains. In such regions, sediment deposition is expected to be lower, considering the higher velocity of the river flow [61]. Moreover, from experience and community feedback in Kaldar District, the sediment deposition is known to be negligible in this area.

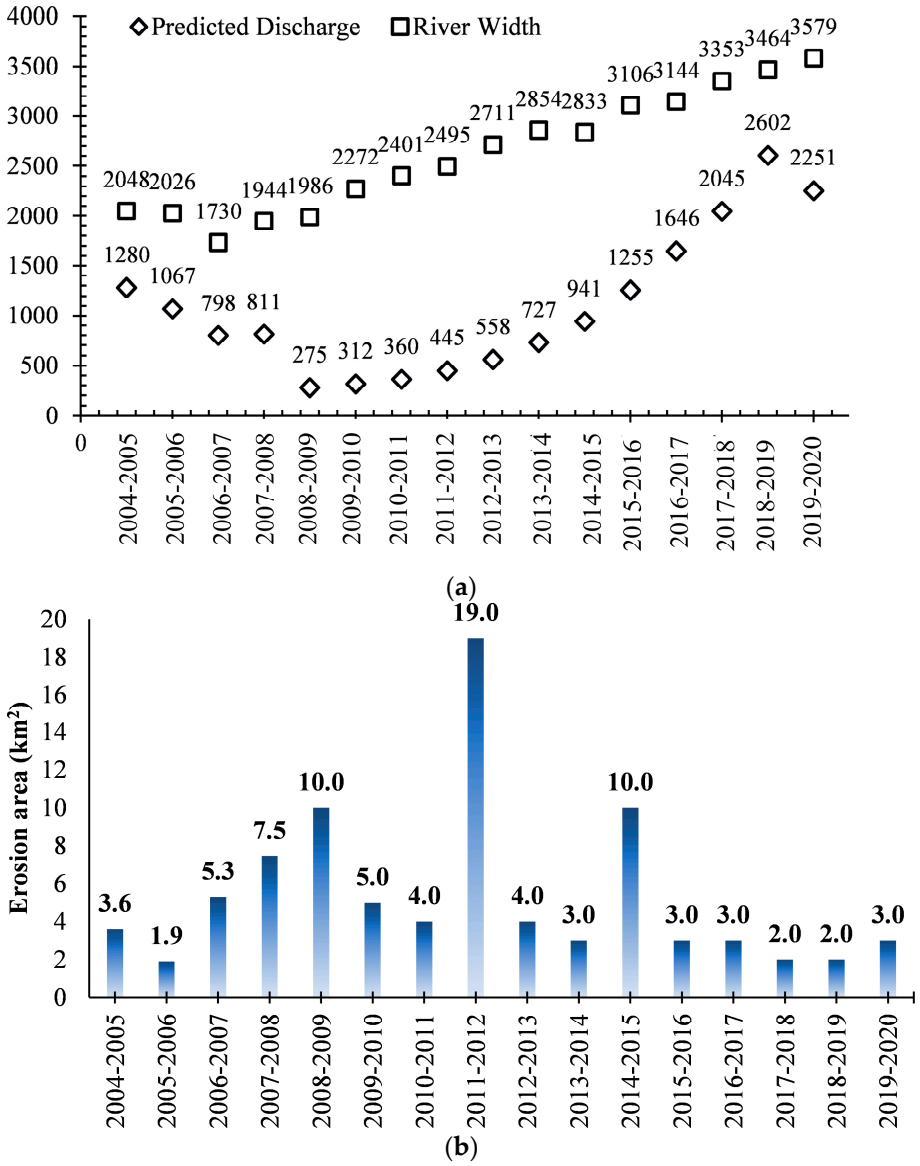

Figure 8. (**a**) Shows the annual mean predicted discharge and river width determined from ERA5 Reanalysis and Landsat-8 data, respectively. (**b**) Shows the annual land loss with peak occurrences in 2009, 2012, and 2015, where extreme flash floods and riverine floods were observed in the Afghanistan side of the study area.

The annual mean erosion area determined from the digital shoreline analysis is shown in Figure 8b, where peak periods are observed in 2009, 2012, and 2015, primarily attributed to the occurrence of flash floods and riverine floods. According to the OCHA [60], high levels of land erosion were observed due to the Amu River riverbanks in Kaldar District of Balkh Province. As a consequence of the riverbank erosion, 145 families lost their homes, gardens, agricultural land, and livelihoods. Further, it was observed that the river shifts due to erosion prevail mostly on the Afghanistan side, as observed in Figure 9. From the digital shoreline analysis, the land loss from the riverbank erosion was observed to be 86.3 km^2 overall between 2004 and 2020, with an annual mean of 5.39 km^2. The peak erosion during this period was observed in 2012, with other significantly large erosion events in 2008, 2010, and 2015.

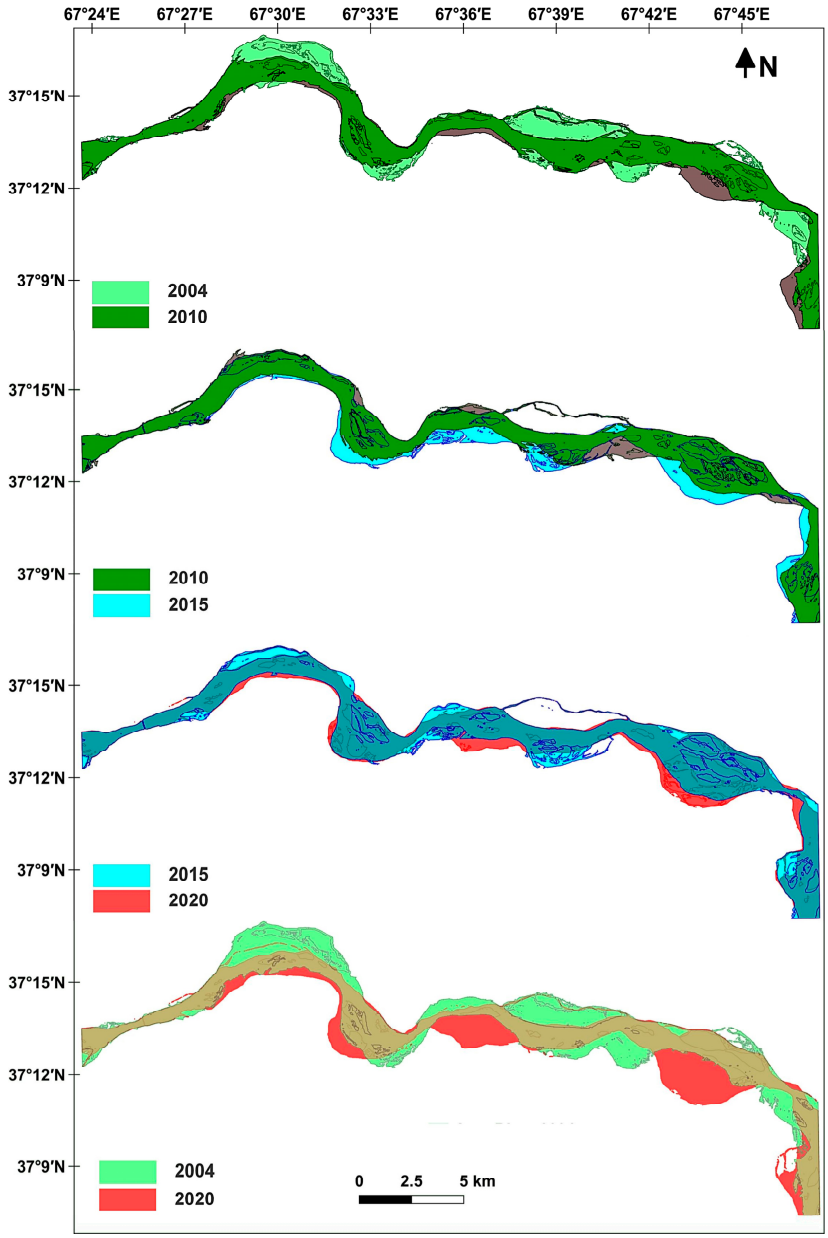

Figure 9. Riverbank shifting due to various factors between 2004 and 2020 in Kaldar District of Balkh Province, Afghanistan, as determined by the digital shoreline analysis. Amu River divides Afghanistan in the south and Uzbekistan in the north in Balkh Province.

4. Conclusions

For developing countries like Afghanistan, resilience against disasters such as floods and riverbank erosion is of utmost significance. Afghanistan has experienced periodical events of flash floods and riverine floods that have caused a significant setback to the overall development of infrastructure in the country. Due to the scarcity of field observations, insights related to river monitoring are primarily constrained. Thus, other means to retrieve significant information for planning and action against such disasters are being sought. The present study focused on the Amu River basin for the assessment of the total land loss towards the Afghanistan side due to riverbank erosion. It was observed that the major factors in the Amu River basin that influence the riverbank erosion are associated with the river discharge, which can be modeled precisely using ERA5 Reanalysis data. The prediction models could be further improved when field information is available from Tajikistan based on possible multi-national cooperation between their governments.

Further improvements could be observed in the determination of the flow parameters, such as the specific stream power where the river width measurements are determined, using higher-resolution satellite imagery. In the present study, the expected anomalies in the river discharge corresponding to the peak erosion periods were not observed due to constraints in the prediction model or the river discharge. However, monitoring these anomalies upon joint interventions leading to preparedness for flooding and mass erosion events could be possible.

Author Contributions: Conceptualization, A.B.M., D.V., S.S., H.O., S.A., G.G. and H.O.E.; methodology, A.B.M., S.S., H.O., S.A., G.G., A.E.-Z.M.A.M., H.R. and Y.K.A.; software, A.B.M., D.V., H.O., S.A., G.G. and H.O.E.; validation, D.V., S.S., H.O., A.E.-Z.M.A.M., H.R., Y.K.A. and H.O.E.; formal analysis, investigation, A.B.M., S.A. and G.G.; resources, Y.K.A., H.O.E., A.E.-Z.M.A.M., H.R. and S.S.; data curation, A.B.M., D.V., S.S., H.O., S.A., G.G. and H.O.E.; writing—original draft preparation, A.B.M., D.V., and S.S.; writing—review and editing, D.V., S.S., H.O., A.E.-Z.M.A.M., H.R., Y.K.A. and H.O.E.; visualization, A.B.M., S.A. and G.G., funding acquisition, S.A., G.G., A.E.-Z.M.A.M., H.R., Y.K.A. and H.O.E. All authors have read and agreed to the published version of the manuscript.

Funding: Researchers' Supporting Project number (RSPD2023R1048), King Saud University.

Data Availability Statement: The data used in this study are freely available to the scientific community except for the ground station data. The authors would like to mention that the ground station data used in this study correspond to sensitive locations and are available only from General Directorate of Water Resources, National Water Affairs Regulation Authority (GMSGA, https://nwara.gov.af/en), and any requests for these data can be made directly to GMSGA. The authors would like to mention that the ERA5 Reanalysis data could be downloaded from the Copernicus Climate Data Store (https://cds.climate.copernicus.eu/), and the Landsat images are available from the EarthExplorer portal of the USGS at https://earthexplorer.usgs.gov/. The shapefiles of the Amu River are shifting.

Acknowledgments: The authors appreciate Researchers' Supporting Project number (RSPD2023R1048), King Saud University, Riyadh, Saudi Arabia. We also acknowledge Vinay Chembolu for his valuable suggestions regarding this work. The authors also thank the General Directorate of Water Resources, National Water Affairs Regulation Authority (GMSGA), Afghanistan, for providing the ground station data corresponding to ERA5 Reanalysis data. We would also like to thank the United Nations Office for Coordination of Humanitarian Affairs (UNOCHA, https://data.humdata.org/) and Centre for Research on the Epidemiology of Disasters—CRED, Université Catholique de Louvain (https://cred.be/projects/EM-DAT) for providing the disaster-related data.

Conflicts of Interest: The authors declare that there is no conflict of interest.

References

1. Langat, P.K.; Kumar, L.; Koech, R. Monitoring river channel dynamics using remote sensing and GIS techniques. *Geomorphology* **2019**, *325*, 92–102. [CrossRef]
2. Paul, B.K.; Rahman, M.K.; Crawford, T.; Curtis, S.; Miah, M.G.; Islam, M.R.; Islam, M.S. Explaining mobility using the Community Capital Framework and Place Attachment concepts: A case study of riverbank erosion in the Lower Meghna Estuary, Bangladesh. *Appl. Geogr.* **2020**, *125*, 102199. [CrossRef]
3. Kumer, R.D.; Goswami, S.; Ahmed, T.; Kumar, S.M.; Hasan, E.M.; Abdur, R.M. SocioEconomic Impacts of River Bank Erosion on Durgapasha Union in Bakerganj Upazila, Bangladesh. *Barisal Univ. J. Part 1* **2017**, *4*, 165–183.
4. Mukhopadhyay, A.; Ghosh, P.; Chanda, A.; Ghosh, A.; Ghosh, S.; Das, S.; Ghosh, T.; Hazra, S. Threats to coastal communities of Mahanadi delta due to imminent consequences of erosion—Present and near future. *Sci. Total Environ.* **2018**, *637–638*, 717–729. [CrossRef]
5. Mahantesh, K.K.; Prashanth, P.; Chandrashekhar, R.; Saidaih, P.; Siddappa; Umesh, B.C. Evaluation of different African marigold (*Tagetes* species Linn.) genotypes for vegetative, floral and yield attributes under Southern Telangana condition. *Int. J. Chem. Stud.* **2018**, *6*, 3311–3315.
6. Rahman, M.; Popke, J.; Crawford, T.W. Resident perceptions of riverbank erosion and shoreline protection: A mixed-methods case study from Bangladesh. *Nat. Hazards* **2022**, *114*, 2767–2786. [CrossRef]
7. Debnath, J.; Sahariah, D.; Lahon, D.; Nath, N.; Chand, K.; Meraj, G.; Kumar, P.; Singh, S.K.; Kanga, S.; Farooq, M. Assessing the impacts of current and future changes of the planforms of river Brahmaputra on its land use-land cover. *Geosci. Front.* **2023**, *14*, 101557. [CrossRef]
8. Das, T.K.; Haldar, S.K.; Das Gupta, I.; Sen, S. River Bank Erosion Induced Human Displacement and Its Consequences. *Living Rev. Landsc. Res.* **2014**, *8*, 3. [CrossRef]

9. Sarif, M.N.; Siddiqui, L.; Siddiqui, M.A.; Parveen, N.; Islam, M.S.; Khan, S.; Khanam, N.; Mohibul, S.; Shariq, M.; Nasrin, T. Household-Based Approach to Assess the Impact of River Bank Erosion on the Socio-economic Condition of People: A Case Study of Lower Ganga Plain. In *Challenges of Disasters in Asia*; Sajjad, H., Siddiqui, L., Rahman, A., Tahir, M., Siddiqui, M.A., Eds.; Springer: Singapore, 2022; pp. 73–101. ISBN 978-981-19-3567-1.
10. Baki, A.B.M.; Gan, T.Y. Riverbank migration and island dynamics of the braided Jamuna River of the Ganges–Brahmaputra basin using multi-temporal Landsat images. *Quat. Int.* **2012**, *263*, 148–161. [CrossRef]
11. Anh, H.H.; Thuy, N.N. Socio-economic assessment of riverbank erosion from heavy boat traffic: A case study at the Cho Gao Canal, Tien Giang, Vietnam. *IOP Conf. Ser. Earth Environ. Sci.* **2022**, *967*, 12005. [CrossRef]
12. Mahmoodzada, A.B.; Shimada, S.; Azizi, M.; Hqbin, M.; Mahmoodzada, A.S. Monitoring of Riverbank Erosion and Shoreline Movement at Amu River Using Remote Sensing and GIS: A Case Study in Jowzjan, Afghanistan. *Int. J. Environ. Rural. Dev.* **2019**, *10*, 140–145. [CrossRef]
13. Baymanov, K.I.; Uzakov, T.J.; Baimanov, R.K.; Tajibaev, S. Riverbed processes in the lower reaches of the Amu Darya river in conditions of anthropogenic impact on the river flow. *IOP Conf. Ser. Earth Environ. Sci.* **2022**, *1045*, 12002. [CrossRef]
14. Wright, J.M. *Floodplain Management Principles and Current Practices*; University of Tennessee: Knocksville, TN, USA, 2007.
15. Longoni, L.; Papini, M.; Brambilla, D.; Barazzetti, L.; Roncoroni, F.; Scaioni, M.; Ivanov, V.I. Monitoring Riverbank Erosion in Mountain Catchments Using Terrestrial Laser Scanning. *Remote Sens.* **2016**, *8*, 241. [CrossRef]
16. Torres, R.; Snoeij, P.; Geudtner, D.; Bibby, D.; Davidson, M.; Attema, E.; Potin, P.; Rommen, B.; Floury, N.; Brown, M.; et al. GMES Sentinel-1 mission. *Remote Sens. Environ.* **2012**, *120*, 9–24. [CrossRef]
17. Awasthi, S.; Varade, D. Recent advances in the remote sensing of alpine snow: A review. *GIScience Remote Sens.* **2021**, *58*, 852–888. [CrossRef]
18. Rahman, M.A.T.; Islam, S.; Rahman, S.H. Coping with flood and riverbank erosion caused by climate change using livelihood resources: A case study of Bangladesh. *Clim. Dev.* **2014**, *7*, 185–191. [CrossRef]
19. Welty, J.; Zeng, X. Characteristics and Causes of Extreme Snowmelt over the Conterminous United States. *Bull. Am. Meteorol. Soc.* **2021**, *102*, E1526–E1542. [CrossRef]
20. Singh, H.; Varade, D.; van Vries, M.W.d.; Adhikari, K.; Rawat, M.; Awasthi, S.; Rawat, D. Assessment of potential present and future glacial lake outburst flood hazard in the Hunza valley: A case study of Shisper and Mochowar glacier. *Sci. Total Environ.* **2023**, *868*, 161717. [CrossRef]
21. Singh, H.; Varade, D.; Mishra, P.K. Cloudburst Events in the Indian Himalayas: A Historical Geospatial Perspective. In *International Handbook of Disaster Research*; Singh, A., Ed.; Springer: Singapore, 2022; pp. 1–21, ISBN 978-981-16-8800-3.
22. Lam-Dao, N.; Viet, P.-B.; Minh, N.-T.; Mai-Thy, P.-T.; Phung, H.-P. Change Detection of Land Use and Riverbank in Mekong Delta, Vietnam Using Time Series Remotely Sensed Data. *J. Resour. Ecol.* **2011**, *2*, 370. [CrossRef]
23. Sun, C.; Hou, H.; Chen, W. Effects of vegetation cover and slope on soil erosion in the Eastern Chinese Loess Plateau under different rainfall regimes. *PeerJ* **2021**, *9*, e11226. [CrossRef]
24. Zhao, J.; Feng, X.; Deng, L.; Yang, Y.; Zhao, Z.; Zhao, P.; Peng, C.; Fu, B. Quantifying the Effects of Vegetation Restorations on the Soil Erosion Export and Nutrient Loss on the Loess Plateau. *Front. Plant Sci.* **2020**, *11*, 573126. [CrossRef] [PubMed]
25. Frotan, M.S.; Nakaza, E.; Schaab, C.; Motoyashiki, R. Surface water resources of Afghanistan's northern River basin and effects of climate change. *J. JSCE* **2020**, *8*, 118–126. [CrossRef] [PubMed]
26. OCHA Services. Afghanistan: Overview of Natural Disasters. 2021. Available online: https://response.reliefweb.int/afghanistan/natural-disasters-dashboard (accessed on 10 September 2023).
27. Henshaw, A.J.; Thorne, C.R.; Clifford, N.J. Identifying causes and controls of river bank erosion in a British upland catchment. *CATENA* **2013**, *100*, 107–119. [CrossRef]
28. Ahmad, M.; Wasiq, M. *Water Resource Development in Northern Afghanistan and Its Implications for Amu Darya Basin*; World Bank: Washington, DC, USA, 2004; ISBN 0-8213-5890-1.
29. Tarek, M.; Brissette, F.P.; Arsenault, R. Evaluation of the ERA5 reanalysis as a potential reference dataset for hydrological modelling over North America. *Hydrol. Earth Syst. Sci.* **2020**, *24*, 2527–2544. [CrossRef]
30. Muñoz-Sabater, J.; Dutra, E.; Agustí-Panareda, A.; Albergel, C.; Arduini, G.; Balsamo, G.; Boussetta, S.; Choulga, M.; Harrigan, S.; Hersbach, H.; et al. ERA5-Land: A state-of-the-art global reanalysis dataset for land applications. *Earth Syst. Sci. Data* **2021**, *13*, 4349–4383. [CrossRef]
31. Dembélé, M.; Ceperley, N.; Zwart, S.J.; Salvadore, E.; Mariethoz, G.; Schaefli, B. Potential of satellite and reanalysis evaporation datasets for hydrological modelling under various model calibration strategies. *Adv. Water Resour.* **2020**, *143*, 103667. [CrossRef]
32. Mahto, S.S.; Mishra, V. Does ERA-5 Outperform Other Reanalysis Products for Hydrologic Applications in India? *J. Geophys. Res. Atmos.* **2019**, *124*, 9423–9441. [CrossRef]
33. Mahmoodzada, A.B.; Varade, D.; Shimada, S.; Okazawa, H.; Vinay, C. Average Quantifying the Snowmelt Dominant River Erosion in Afghanistan between 2004–2020. In Proceedings of the EGU21-10888, EGU General Assembly, Online, 19–30 April 2021.
34. Hagg, W.; Hoelzle, M.; Wagner, S.; Mayr, E.; Klose, Z. Glacier and runoff changes in the Rukhk catchment, upper Amu-Darya basin until 2050. *Glob. Planet. Chang.* **2013**, *110*, 62–73. [CrossRef]
35. Agal'tseva, N.A.; Bolgov, M.V.; Spektorman, T.Y.; Trubetskova, M.D.; Chub, V.E. Estimating hydrological characteristics in the Amu Darya River basin under climate change conditions. *Russ. Meteorol. Hydrol.* **2011**, *36*, 681–689. [CrossRef]

36. Mahmoodzada, A.B.; Varade, D.; Shimada, S. Estimation of Snow Depth in the Hindu Kush Himalayas of Afghanistan during Peak Winter and Early Melt Season. *Remote Sens.* **2020**, *12*, 2788. [CrossRef]
37. Mahmoodzada, A.B.; Varade, D.; Shimada, S.; Rezazada, F.A.; Mahmoodzada, A.S.; Jawher, A.N.; Toghyan, M. Capability assessment of Sentinel-1 data for estimation of snow hydrological potential in the Khanabad watershed in the Hindu Kush Himalayas of Afghanistan. *Remote Sens. Appl. Soc. Environ.* **2022**, *26*, 100758. [CrossRef]
38. Matveeva, T.; Sidorchuk, A. Modelling of Surface Runoff on the Yamal Peninsula, Russia, Using ERA5 Reanalysis. *Water* **2020**, *12*, 2099. [CrossRef]
39. Tha, T.; Piman, T.; Bhatpuria, D.; Ruangrassamee, P. Assessment of Riverbank Erosion Hotspots along the Mekong River in Cambodia Using Remote Sensing and Hazard Exposure Mapping. *Water* **2022**, *14*, 1981. [CrossRef]
40. Bhatpuria, D.; Matheswaran, K.; Piman, T.; Tha, T.; Towashiraporn, P. Assessment of Large-Scale Seasonal River Morphological Changes in Ayeyarwady River Using Optical Remote Sensing Data. *Remote Sens.* **2022**, *14*, 3393. [CrossRef]
41. Mu, X.; Qiu, J.; Cao, B.; Cai, S.; Niu, K.; Yang, X. Mapping Soil Erosion Dynamics (1990–2020) in the Pearl River Basin. *Remote Sens.* **2022**, *14*, 5949. [CrossRef]
42. Sil, B.S.; Ashwini, K.; Annayat, W.; Debnath, J.; Farooq, M.; Meraj, G. Observing Spatiotemporal Inconsistency of Erosion and Accretion in the Barak River Using Remote Sensing and GIS Techniques. *Conservation* **2023**, *3*, 14–31. [CrossRef]
43. Wilson, Z.A.; Song, J.; Taylor, B.; Yang, C. The final split: The regulation of anther dehiscence. *J. Exp. Bot.* **2011**, *62*, 1633–1649. [CrossRef]
44. Chen, Y.; Sun, K.; Li, D.; Bai, T.; Huang, C. Radiometric Cross-Calibration of GF-4 PMS Sensor Based on Assimilation of Landsat-8 OLI Images. *Remote Sens.* **2017**, *9*, 811. [CrossRef]
45. De Rosa, P.; Fredduzzi, A.; Cencetti, C. Stream Power Determination in GIS: An Index to Evaluate the Most 'Sensitive'Points of a River. *Water* **2019**, *11*, 1145. [CrossRef]
46. World Bank Group. Afghanistan-Irrigation Restoration and Development (IRD) Project. Report No: 58454-AF. Available online: https://documents1.worldbank.org/curated/en/598691468198013735/pdf/584540PJPR0P121OFFICIAL0USE0ONLY191.pdf (accessed on 10 September 2023).
47. Xu, S.; Ehlers, M. Hyperspectral Image Sharpening Based on Ehlers Fusion. *Int. Arch. Photogramm. Remote Sens. Spat. Inf. Sci.* **2017**, *42*, 941–947. [CrossRef]
48. Ehlers, M.; Klonus, S.; Åstrand, P.J.; Rosso, P. Multi-sensor image fusion for pansharpening in remote sensing. *Int. J. Image Data Fusion* **2010**, *1*, 25–45. [CrossRef]
49. Chachondhia, P.; Shakya, A.; Kumar, G. Performance evaluation of machine learning algorithms using optical and microwave data for LULC classification. *Remote Sens. Appl. Soc. Environ.* **2021**, *23*, 100599. [CrossRef]
50. Yin, G.; Mariethoz, G.; McCabe, M. Gap-Filling of Landsat 7 Imagery Using the Direct Sampling Method. *Remote Sens.* **2017**, *9*, 12. [CrossRef]
51. Himmelstoss, E.A.; Henderson, R.E.; Kratzmann, M.G.; Farris, A.S. *Digital Shoreline Analysis System (DSAS) Version 5.0 User Guide*; Report 2018-1179; USGS: Reston, VA, USA, 2018. Available online: http://pubs.er.usgs.gov/publication/ofr20181179 (accessed on 10 September 2023).
52. Akbary, S.M. *A Glance to Vulnerable Areas in Panj River in Takhar Province: Internal Report*; Directorate of the Taliqan River Basin, Ministry of Water Resource Management: Kabul, Afghanistan, 2020.
53. Hersbach, H.; Bell, B.; Berrisford, P.; Hirahara, S.; Horányi, A.; Muñoz-Sabater, J.; Nicolas, J.; Peubey, C.; Radu, R.; Schepers, D.; et al. The ERA5 global reanalysis. *Q. J. R. Meteorol. Soc.* **2020**, *146*, 1999–2049. [CrossRef]
54. Kraatz, S.; Khanbilvardi, R.; Romanov, P. A Comparison of MODIS/VIIRS Cloud Masks over Ice-Bearing River: On Achieving Consistent Cloud Masking and Improved River Ice Mapping. *Remote Sens.* **2017**, *9*, 229. [CrossRef]
55. Nain, S.; Beniwal, B.S.; Dalal, R.P.S.; Sheoran, S. Effect of pinching and spacing on growth, flowering and yield of African marigold (*Tagetes erecta* L.) under semi-arid conditions of Haryana. *J. Appl. Nat. Sci.* **2017**, *9*, 2073–2078. [CrossRef]
56. CRED. Emergency Events Database. Centre for Research on Epidemology of Disasters (CRED), UC Louvain. Available online: https://cred.be/projects/EM-DAT (accessed on 22 January 2021).
57. Lucianetti, G.; Penna, D.; Mastrorillo, L.; Mazza, R. The Role of Snowmelt on the Spatio-Temporal Variability of Spring Recharge in a Dolomitic Mountain Group, Italian Alps. *Water* **2020**, *12*, 2256. [CrossRef]
58. López-Moreno, J.I.; García-Ruiz, J.M. Influence of snow accumulation and snowmelt on streamflow in the central Spanish Pyrenees/Influence de l'accumulation et de la fonte de la neige sur les écoulements dans les Pyrénées centrales espagnoles. *Hydrol. Sci. J.* **2009**, *49*, 478. [CrossRef]
59. Fassnacht, S.R.; Records, R.M. Large snowmelt versus rainfall events in the mountains. *J. Geophys. Res. Atmos.* **2015**, *120*, 2375–2381. [CrossRef]
60. Humdata-UNOCHA. The Humanitarian Data Exchange. Available online: https://data.humdata.org/ (accessed on 22 January 2021).
61. Akhundzadah, N.A.; Soltani, S.; Aich, V. Impacts of Climate Change on the Water Resources of the Kunduz River Basin, Afghanistan. *Climate* **2020**, *8*, 102. [CrossRef]

Disclaimer/Publisher's Note: The statements, opinions and data contained in all publications are solely those of the individual author(s) and contributor(s) and not of MDPI and/or the editor(s). MDPI and/or the editor(s) disclaim responsibility for any injury to people or property resulting from any ideas, methods, instructions or products referred to in the content.